Structural and functional studies of Bud23–Trm112 reveal 18S rRNA N^7-G1575 methylation occurs on late 40S precursor ribosomes

Juliette Létoquart[a,1], Emmeline Huvelle[b,1], Ludivine Wacheul[c,1], Gabrielle Bourgeois[a], Christiane Zorbas[c], Marc Graille[a,2], Valérie Heurgué-Hamard[b,2], and Denis L. J. Lafontaine[c,d,2]

[a]Laboratoire de Biochimie, CNRS UMR 7654, Ecole Polytechnique, F-91128 Palaiseau Cedex, France; [b]CNRS FRE3630 (affiliated with Université Paris Diderot, Sorbonne Paris Cité), Institut de Biologie Physico-Chimique, Paris F-75005, France; [c]Center for Microscopy and Molecular Imaging, B-6041 Charleroi-Gosselies, Belgium; and [d]RNA Molecular Biology, Fonds de la Recherche Scientifique, Université Libre de Bruxelles, B-6041 Charleroi-Gosselies, Belgium

The eukaryotic small ribosomal subunit carries only four ribosomal (r) RNA methylated bases, all close to important functional sites. N^7-methylguanosine (m^7G) introduced at position 1575 on 18S rRNA by Bud23–Trm112 is at a ridge forming a steric block between P- and E-site tRNAs. Here we report atomic resolution structures of Bud23–Trm112 in the apo and S-adenosyl-L-methionine (SAM)-bound forms. Bud23 and Trm112 interact through formation of a β-zipper involving main-chain atoms, burying an important hydrophobic surface and stabilizing the complex. The structures revealed that the coactivator Trm112 undergoes an induced fit to accommodate its methyltransferase (MTase) partner. We report important structural similarity between the active sites of Bud23 and Coffea canephora xanthosine MTase, leading us to propose and validate experimentally a model for G1575 coordination. We identify Bud23 residues important for Bud23–Trm112 complex formation and recruitment to pre-ribosomes. We report that though Bud23–Trm112 binds precursor ribosomes at an early nucleolar stage, m^7G methylation occurs at a late step of small subunit biogenesis, implying specifically delayed catalytic activation. Finally, we show that Bud23–Trm112 interacts directly with the box C/D snoRNA U3-associated DEAH RNA helicase Dhr1 supposedly involved in central pseudoknot formation; this suggests that Bud23–Trm112 might also contribute to controlling formation of this irreversible and dramatic structural reorganization essential to overall folding of small subunit rRNA. Our study contributes important new elements to our understanding of key molecular aspects of human ribosomopathy syndromes associated with WBSCR22 (human Bud23) malfunction.

ribosome synthesis | rRNA modifying enzyme | methyltransferase | translation | S-adenosyl-L-methionine

In living cells, all proteins are synthesized by ribosomes, consisting in eukaryotes of four rRNAs and 80 ribosomal proteins. Synthesizing these nanomachines is a complex multistep process involving at least 200 assembly factors and dozens of small nucleolar RNAs (snoRNAs) (1, 2). Ribosome assembly factors are recruited to incipient ribosomes in a controlled stepwise and dynamic process (3), and they are required for the synthesis, maturation, transport, and assembly of ribosomal components. Maturation of components includes pre-rRNA processing (generation of the 5′ and 3′ termini of mature rRNA from long precursor molecules) and RNA modification (selection of specific rRNA residues during subunit biogenesis for covalent modification). rRNA processing and modification are highly coordinated processes (4).

Methylation is a prevalent posttranscriptional rRNA modification, occurring either on riboses or bases (5). Ribose methylation is essentially performed by box C/D snoRNA-guided enzymes (6), whereas base methylations are specifically catalyzed by standalone protein-only methyltransferases, which are highly conserved from yeast to metazoans (7–9). Base methylation is thought to contribute to expanding the structural repertoire of RNA, promoting

base stacking through increased hydrophobicity or altering steric hindrance (10). rRNA base MTases use S-adenosyl-L-methionine (SAM) as a methyl donor, and most have been shown or predicted to belong to class I, containing the characteristic Rossmann-like fold domain (11).

In budding yeast, six base methylations have been inventoried on the large subunit, on the 25S rRNA. The six enzymes involved, Bmt2, Bmt5, Bmt6, Nop2, Rcm1, and Rrp8, have only been identified recently (12–15); of these, only Nop2 (responsible for m^5C_{2870}) is essential to growth, whereas loss of any of the others, including Bmt2 (m^1A_{2142}), Bmt5 (m^3U_{2634}), Bmt6 (m^3U_{2843}), Rcm1 (m^5C_{2278}), and Rrp8 (m^1A_{645}), does not impair cell growth significantly (12–15). The small subunit 18S rRNA contains one hypermodified base: m^1-aminocarboxypropyl(acp)^3-Ψ_{1191}, which is methylated at the N^1 position by Nep1 (Emg1) (16), two contiguous dimethylated adenosines $m^6_2A_{1781}m^6_2A_{1782}$, modified at N^6 by Dim1 (7), and one methylated guanosine m^7G_{1575}, methylated at N^7 by the Bud23–Trm112 complex (8, 17, 18). In contrast to the majority of large subunit MTases, deletion of genes encoding modification enzymes specific to the small ribosomal

Significance

Ribosomes are essential cellular nanomachines responsible for all protein synthesis in vivo. Efficient and faithful ribosome biogenesis requires a plethora of assembly factors whose precise role and timing of action remains to be established. Here we determined the crystal structure of Bud23–Trm112, which is required for efficient pre-rRNA processing steps leading to 18S rRNA synthesis and methylation of 18S rRNA at position G1575. For the first time, to our knowledge, we identified where on Bud23–Trm112 the contacts with precursor ribosomes occur. We further report that the essential helicase Dhr1 interacts directly with Bud23–Trm112, proposing a concerted action of these proteins in ribosome assembly. Finally, we reveal that the methyltransferase activity of Bud23–Trm112 and its requirement for pre-rRNA processing are disconnected in time.

subunit is lethal (Nep1, Dim1) or affects cell growth drastically (Bud23–Trm112) (7–9, 19). Surprisingly, however, the analysis of catalytically dead methyltransferase mutants has revealed it is the protein itself, rather than its enzymatic activity in RNA methylation, that is essential to subunit biogenesis, and in particular for pre-rRNA processing (7–9, 19). Nonetheless, these base methylations all cluster at functionally important and highly conserved sites on the ribosome, suggesting possible roles in translation.

Recently we demonstrated that Bud23 is active in 18S rRNA N^7G methylation as a heterodimer in a complex with Trm112 (17). Trm112 is a small zinc finger protein that interacts with and activates three class I MTases in addition to Bud23; these are all related to translation and include Mtq2, which methylates the translation termination factor eRF1, and Trm9 and Trm11, which both modify tRNAs (20–22). Trm112 is required for Bud23 metabolic stability and hence for Bud23-mediated methylation of 18S rRNA and efficient small subunit synthesis (17). Bud23–Trm112 binds early nucleolar pre-ribosomes and could act at the time of A$_2$ cleavage (17). Genetic interactions suggest that Bud23 might be involved in disassembly of the small subunit processome (18), a large ribonucleoprotein complex corresponding to nascent pre-40S ribosomes that have undergone initial U3 snoRNA-dependent pre-rRNA cleavages (23). More recently, Bud23 was reported to interact physically and functionally with the DEAH box helicase Dhr1 (24), also required for processing at cleavage site A$_2$ and with a predicted role in central pseudoknot formation (25).

Human Bud23, known as WBSCR22 (or MERM1), is also required for 40S subunit biogenesis and 18S rRNA G1575 methylation (26, 27). WBSCR22 has been identified as a cancer metastasis promoter, a breast cancer biomarker, and a putative therapeutic target in myeloma (28, 29). WBSCR22 is also one of the multiple genes associated with the neurodevelopmental disorder William–Beuren syndrome (30).

More than 200 ribosome assembly factors have been identified in budding yeast, though their precise role in subunit biogenesis remains largely to be elucidated. Here we have combined structural and functional approaches to characterize the 18S rRNA MTase Bud23–Trm112. We report essential features of methylation catalysis, including most importantly an experimentally validated model for guanosine substrate coordination in the catalytic pocket of Bud23, and the requirement for an induced fit in the coactivator Trm112 to achieve complex formation and stabilization. We further report that Bud23–Trm112 interacts directly with the U3 snoRNA-associated helicase Dhr1, forming in vitro a trimeric complex. This observation offers novel important insights into the involvement of Bud23–Trm112 in small subunit biogenesis. Finally, we provide a methylation timetable, demonstrating that m^{7}G occurs at a late stage of subunit assembly, and Bud23–Trm112 is recruited to pre-ribosomes at an early nucleolar step; this implies specifically delayed catalytic activation.

Materials and Methods

Detailed experimental procedures are available in *SI Materials and Methods*.

Cloning, Production, and Purification of the Dhr1 [58–270] Domain. Plasmid pVH481 (Table S1) encoding the full-length *Saccharomyces cerevisiae* DHR1 gene was used as template to amplify the DNA region encoding the Dhr1 [58–270] domain with primers oMG205 and oMG206 (Table S2). The PCR amplicon was digested with BglII and XhoI (Fermentas) and cloned into pGEX-6P-1 (BamHI–XhoI) to yield plasmid pMG679. The various plasmids, oligonucleotides and strains used in this study are presented in Tables S1–S5.

The GST-Dhr1 [58–270] protein was expressed at 37 °C for 3 h, following induction with 0.5 mM IPTG, in a transformed *Escherichia coli* BL21(DE3) Gold strain cultured in 1 L of 2xYT medium. Cells were harvested and resuspended in 20 mM Tris·HCl (pH 7.5), 200 mM NaCl. The protein was purified on a Glutathione Sepharose 4B resin (GE Healthcare) and eluted with the same buffer supplemented with 20 mM reduced glutathione. GST was cleaved from the Dhr1 [58–270] domain by overnight incubation with

GST-3C protease (100 µg/L of culture) under dialysis against 20 mM Tris·HCl (pH 7.5), 200 mM NaCl, 5 mM β-mercaptoethanol to remove the glutathione. Cleaved GST, uncleaved GST-Dhr1, and GST-3C protease were removed by incubating the eluate with Glutathione Sepharose 4B resin. The Dhr1 [58–270] protein present in the unbound fraction was further purified by ion-exchange chromatography on a HiTrap SP HP 5-mL (GE Healthcare) column followed by size-exclusion chromatography on a Superdex 75 16/60 column (GE Healthcare) preequilibrated with 20 mM Tris·HCl (pH 7.5), 50 mM NaCl.

Reconstitution of Dhr1–Bud23–Trm112 Ternary Complex. The complex was reconstituted by mixing Bud23–Trm112 with a 1.5 M excess of Dhr1 [58–270] in 20 mM Tris·HCl (pH 7.5), 50 mM NaCl, 10 µM ZnCl$_2$, 5 mM β-mercaptoethanol. The ternary complex was injected on Superdex 200 10/300 GL (GE Healthcare) equilibrated with the same buffer.

Results and Discussion

An Induced Fit in Trm112 Is Necessary to Accommodate the Methyltransferase Bud23. The crystal structure of the complex between Trm112 and the Bud23 MTase domain (residues 1–202) from *S. cerevisiae* (referred to hereafter as Bud23–Trm112) was determined in the absence and presence of SAM cofactor at 2 Å and 2.2 Å resolution, respectively (Table S6). The structures of the apo and SAM-bound forms of the complex are very similar (rmsd value of 0.2 Å). The Bud23 MTase domain adopts a typical class I SAM-dependent MTase fold composed of a central seven-stranded β-sheet flanked by four α-helices on one side (αY, αZ, αA, and αB) and two on the other (αD and αE; Fig. 1*A* and Fig. S1*A*). SAM binds Bud23 in a canonical manner compared with class I SAM-dependent MTases, i.e., at the C-terminal extremity of the central seven-stranded β-sheet (*SI Results and Discussion*). Upon SAM binding, residues I12–H20 and A126–N131 of Bud23 become ordered (Fig. 1*B*). Residues K21–G24, which adopt an extended conformation in the absence of SAM, rearrange so as to expand helix αY by four residues. As a result, the N-terminal residues (residues 12–15) fold as an extended loop followed by helix αY (residues 16–24), which lies on the SAM cofactor. Finally, the W122 side chain, adopting two alternate conformations in the apo structure, is locked in a single conformation upon SAM binding (Fig. 1*B*).

Trm112 is composed of a zinc-binding domain formed by the N- and C-terminal extremities of the protein and consisting of an α-helix (α1) packed against a four-stranded antiparallel β-sheet, as well as a central helical domain (helices α2–α4; Fig. 1*A* and Fig. S1*B*). The structures of Trm112 alone and in the complex are very similar (rmsd value of 0.9 Å) (20). However, a slight rigid body rotation of the Trm112 central domain relative to the zinc-binding domain is observed to accommodate Bud23 in the Trm112–Bud23 complex, compared with the structure of the Trm112 protein alone. Another important difference is observed for Trm112 residues 128–136, which drastically rearrange in the complex upon rotation of the peptide bond connecting N127 to L128 so as to avoid steric clashes with Bud23. A similar rearrangement was previously described for the corresponding region from *Encephalitozoon cuniculi* Trm112 in the complex with Mtq2 (*Ec*Mtq2-Trm112) (31). Hence, we conclude that Trm112 undergoes an induced fit to accommodate Bud23. Because similar rearrangements were described in other Trm112-MTase complexes in other species, we suggest this induced fit is conserved to adapt Trm112 to its multiple MTase partners.

Formation of the Bud23–Trm112 Complex Is Required for Efficient 18S rRNA Maturation. In the Bud23–Trm112 complex, both proteins interact mainly via formation of a parallel β-zipper between Bud23 strand β3 and Trm112 strand β4 to form a remarkable continuous 11-stranded β-sheet (Fig. 1 *A* and *C*). Complex formation involves a large surface area of 1,230 Å^2 formed by 19 and 24 residues of Bud23 and Trm112, respectively. The interface is characterized by the presence of a central large hydrophobic core composed of residues F50, V72, L87, L95, M96, L97, P105, and

Fig. 1. Crystal structures of *S. cerevisiae* Bud23–Trm112 MTase complexes. (*A*) Ribbon representation of the complex between Trm112 (green) and Bud23 (blue). The zinc atom bound to Trm112 is depicted as a dark gray sphere, and the side chains of the cysteine residues coordinating this zinc atom are shown as sticks. The SAM cofactor bound to Bud23 is shown as sticks with carbon atoms shown in light gray. The SAM methyl group (CH₃) transferred during the methylation reaction is shown as a gray sphere. Secondary structure elements of Trm112 are indicated in italics. Bud23 secondary structure elements are annotated according to the nomenclature proposed in ref. 39. (*B*) Conformational changes induced in Bud23 upon SAM binding. Residues I12–G24 from Bud23 are shown in orange as they become ordered (I12–H20) or rearrange to fold as the C-terminal extremity of helix αY (K21–G24) upon SAM binding. The conformation adopted by Bud23 residues K21–G24 in the absence of SAM is shown in magenta. The Bud23 loop encompassing residues A126–N131, which is only visible in the SAM-bound form, is also shown in orange. The side chain of W122, which adopts different conformations in the apo- (magenta) and SAM-bound (blue) structures, is shown as sticks. Bud23 residues involved in SAM binding are shown as sticks, and hydrogen bonds formed between Bud23 residues and SAM are depicted by black dashed lines. Residues mutated in this study are underlined. (*C* and *D*) Detailed views of the interface between Bud23 and Trm112. Residues involved in the interaction are shown as sticks. Electrostatic interactions (hydrogen bonds and salt bridges) are depicted as black dashed lines. Color code as in *A*.

F106 of Bud23 and M1, F8, L9, I40, F46, I50, I125, P126, L128, and L129 of Trm112 (Fig. 1 *C* and *D* and Fig. S1 *A* and *B*). The hydrophobic core at the interface is shielded from the solvent upon complex formation, which explains the stabilizing effect of Trm112 on Bud23 in *S. cerevisiae* cells and why it is required to obtain soluble Bud23 in *E. coli* (17). The hydrophobic interface is surrounded by polar residues involved in the formation of 12 hydrogen bonds and two salt bridges (Table S7). Two hydrogen bonds are formed between the main-chain atoms of residues located in Bud23 strand β3 (L97) and Trm112 strand β4 (P126 and L128) and hence contribute to the formation of the β-zipper interaction (Fig. 1*C*). Among the other polar contacts, two Bud23 residues (D94 and R107) are engaged in five hydrogen bonds with

K2, T5, N7, and R53 residues of Trm112 ((Fig. 1 *C* and *D*). Finally, two salt bridges are involved in the interaction (D112 and R139 of Bud23 with R53 and D17 of Trm112, respectively; Fig. 1*D* and Table S7).

To validate the functional importance of Bud23–Trm112 complex formation in ribosome biogenesis, we mutated three Bud23 residues involved in the interface with Trm112: D94, M96, and D112 (Fig. 1 *C* and *D*). Altogether, five substitutions were introduced at these positions (Table 1). Because Bud23 cannot be expressed as a soluble protein alone (17), we could not use classical in vitro approaches to test the ability of these mutants to interact with Trm112. We reasoned that because deletion of *TRM112* strongly affects Bud23 stability in vivo (17), Bud23 mutants unable

Table 1. Phenotypic analysis of Bud23 mutants

Strains	Growth, DT, min	m⁷G	SAM binding	Protein level (Bud23/PGK1)	Ratio 25S/18S
WT	132	Unaffected	100%	1.0	1.0
bud23Δ	186	Lost	n.d.	0.0	2.3
D94A	204	Unaffected	n.d.	< 0.1	1.1
D94R	257	Unaffected	n.d.	< 0.1	3.3
M96A	134	Unaffected	n.d.	0.6	1.0
D112A	263	Unaffected	n.d.	< 0.1	1.8
D112R	273	Lost	n.d.	< 0.1	3.7
D77A	127	Lost	25% residual	0.6	1.1
E18A	133	Unaffected	n.d.	1.1	0.9
Y22A	124	Lost	Unaffected	1.0	1.1
K21E/R27E	138	Lost	Unaffected	0.8	1.2
I31W	212	Lost	25% residual	0.3	1.1
S118R	136	Lost	Lost	0.5	1.1
S118E	254	Lost	Lost	0.2	1.0
W122A	125	Lost	Unaffected	0.9	1.0
Y159A	124	Lost	50% residual	1.0	1.0

DT, doubling time; n.d., not determined.

to interact with Trm112 should demonstrate decreased stability in yeast cells. The M96A mutant exhibited a modest decrease at protein level and was not associated with any particular phenotype, suggesting that this Bud23 mutant still interacts with Trm112 (Table 1 and Fig. S2*B*). The remaining mutants (D94A, D112A, and the charge inversion mutants D94R and D112R) resulted in strongly impaired Bud23 stability, correlating with a slow-growth defect, similarly to the *bud23Δ* strain (Table 1 and Fig. S2 *A* and *B*) (8). Next, we analyzed the G1575 methylation level in these four mutants. Quite surprisingly, considering the high instability of these Bud23 mutants, only one substitution (D112R) affected methylation (Table 1 and Fig. S2*C*), which indicates that low residual levels of the D94A, D94R, and D112A Bud23 mutants are sufficient to efficiently modify 18S rRNA and suggests that these three mutants are still able to interact with Trm112, most likely in a transient manner. This finding also implies effective recycling of the MTase complex toward nascent pre-ribosomes. Regarding the D112R mutant, we postulate that as D112 forms a salt bridge with R53 of Trm112 (Fig. 1*D*), its replacement by the positively charged arginine induces repulsion between the two proteins and completely precludes complex formation, thereby totally inhibiting 18S rRNA methylation.

Finally, we analyzed the effect of these four mutants on ribosome biogenesis (Table 1 and Fig. S3). As expected from their low protein abundance, three mutants (D94R, D112A, and D112R) exhibited reduced 18S rRNA production. More surprisingly, the unstable D94A mutant did not demonstrate any obvious 18S rRNA production defects, suggesting that it is less affected than the three others. It is noteworthy that substitutions at position D94 affect protein function less than equivalent substitutions at position D112, and that charge inversion mutants display the strongest 18S rRNA maturation defects, suggesting that Ala mutants retain more Trm112 binding activity than Arg mutants; this agrees with a recent report showing that the Bud23 D94G mutant retains the ability to bind to Trm112, whereas D112G does not (24).

G1575 Is Coordinated by a Network of Conserved Bud23 Residues. Mapping sequence conservation at the surface of Bud23–Trm112 revealed a highly conserved, positively charged area surrounding the cavity where the methyl group donor lies (Fig. S4 *A*–*C*). To understand how Bud23 selects and N^7G methylates 18S rRNA at position 1575, we used DALI (32) to search the Protein Data Bank (PDB) for proteins sharing strong structural similarity with Bud23 MTase domain; this identified more than 900 crystal structures of MTases with Z-scores ranging from 20 to

10. Among these structures, a few catalyze N^7 methylation on a purine ring, including *E. coli* ArmA and RmtB (33), *E. cuniculi* mRNA cap guanine N^7-MTase (34), and *Coffea canephora* xanthosine MTase (XMT; rmsd value with Bud23 of 3 Å over 171 Cα atoms, 16% sequence identity (35); *SI Results and Discussion*).

Superimposing the XMT–xanthosine complex onto Bud23 made it possible, to our knowledge for the first time, to propose a robust model for 18S rRNA G1575 coordination in the active site of Bud23 (Fig. 2 *A* and *B*), and this provided important insights into the mode of catalysis and the timing of methylation during ribosome biogenesis. First, many of the XMT residues involved in xanthosine binding are strikingly conserved or replaced by residues with similar properties in Bud23 (Fig. 2*A*): Y22, Q32, Q121, and W122 of Bud23 match, respectively, with Y18, N25, Q161, and W162 of XMT. Second, no steric clashes are observed between the xanthosine purine ring and Bud23 residues. Third, superimposition of the purine ring of GMP onto the xanthosine purine ring reveals that the carbonyl group of the GMP ring could form a direct hydrogen bond with the Q121 side chain and a water-mediated hydrogen bond with the W122 side chain, whereas its purine ring would stack onto Y159 of Bud23 (Fig. 2*B*). In this model, the N^7 atom of GMP is only 2.6 Å away from the SAM methyl group and ideally positioned for methyl transfer by the inline S_N2-type reaction catalyzed by most class I SAM-dependent MTases (11). Finally, to orient the 5′ and 3′ groups of the GMP ribose toward the solvent in a position compatible with accommodating the rRNA around G1575, the ribose moiety has to undergo a rotation relative to the purine ring, bringing its 2′-OH within hydrogen bonding distance to the hydroxyl group of Y159 and to a water molecule present in our crystal structure. This water molecule could mediate the hydrogen bonds connecting the ribose 2′-OH to S118, and Q32 side chains (Fig. 2*B*). In this model, the conserved K21 and R27 of helices αY and αZ are perfectly oriented to interact with the 18S rRNA phosphate backbone, suggesting a possible role for these residues in recruiting Bud23–Trm112 to pre-ribosomes (see below). Furthermore, all residues of Bud23 surrounding GMP in our model are strictly or highly conserved in Bud23 proteins of different species (Fig. S1*A*).

To validate our model, we mutated several strongly conserved Bud23 residues (E18, K21/R27, Y22, I31, S118, W122, and Y159) lining the proposed GMP binding site and analyzed the effect of these mutations on RNA methylation, growth, and rRNA production. Because we have previously shown that Bud23–Trm112 is recruited to nucleolar 90S pre-ribosomes (the first intermediate detected in the assembly pathway and containing the 35S primary
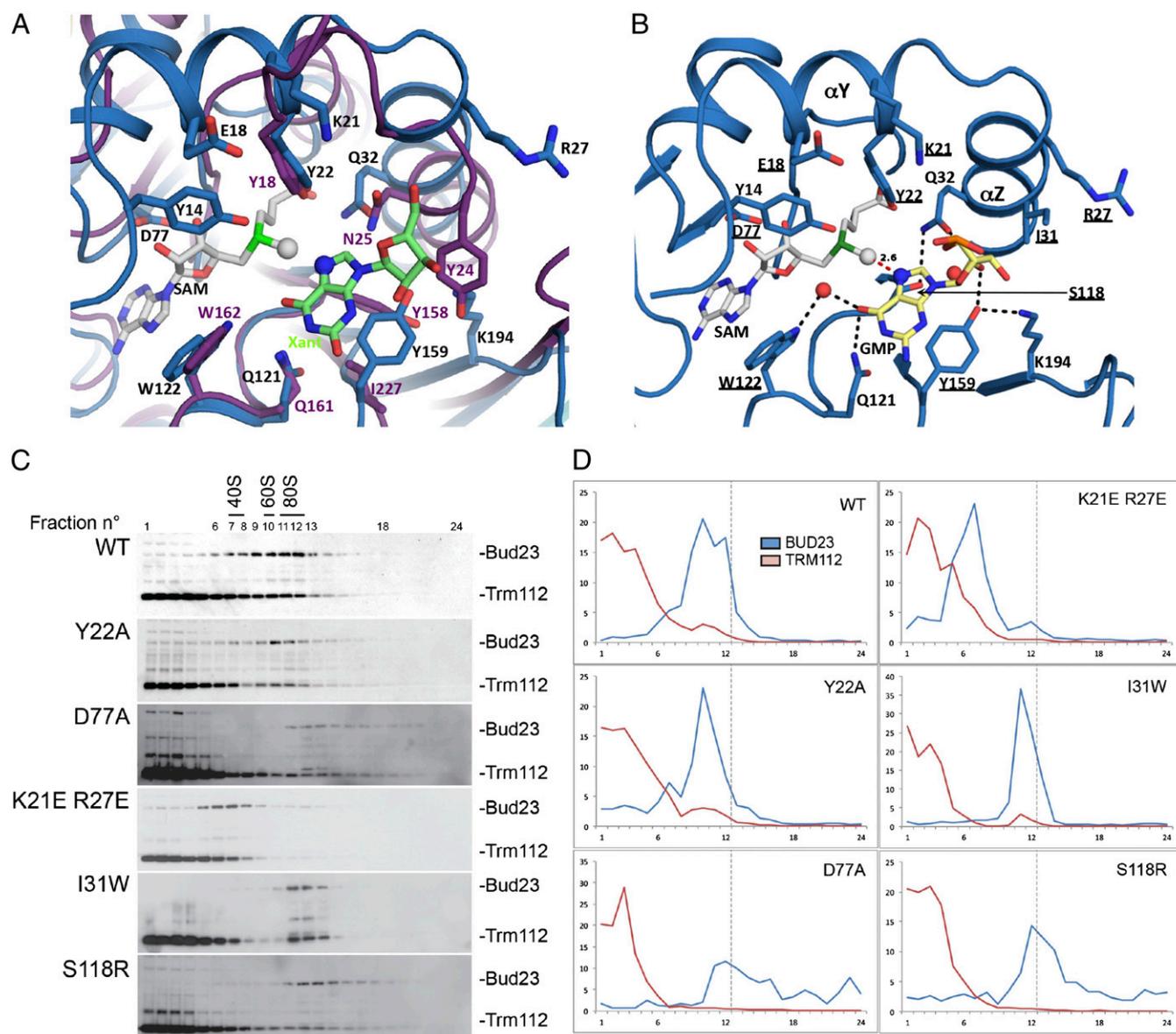
Fig. 2. Bud23 catalytic pocket and interaction of Bud23–Trm112 with pre-ribosomes. (*A*) Superimposition of Bud23 (blue) onto the structure of *C. canephora* xanthosine MTase (purple) (35) bound to xanthosine (Xant; green sticks) and comparison of their active sites. The SAM cofactor bound to Bud23 is shown as sticks with carbon atoms shown in light gray. The SAM methyl group (CH_3) transferred during the methylation reaction is shown as a gray sphere and the recipient N^7 atom by a blue sphere. Important residues of the xanthosine MTase active site and equivalent residues of Bud23 are shown as sticks. (*B*) Model of a GMP molecule (yellow) bound to the Bud23 active site. Model based on the superimposition shown in *A* and generated by superimposing the guanine ring of GMP onto xanthosine. Conserved residues of the Bud23 active site that could be involved in GMP binding are shown as sticks, and hydrogen bonds that these residues could form with GMP are depicted by black dashed lines. The distance between the SAM methyl group (gray sphere) and the guanine N^7 atom (blue sphere) is 2.6 Å and indicated by a red dashed line. Residues mutated in this study are underlined. Water molecules are depicted by red spheres. (*C*) Distribution of Bud23–Trm112 in velocity gradients. Identical amounts of total extract from the indicated strains were resolved on 10–50% sucrose gradients. Total protein extracted from each fraction was collected and analyzed by Western blotting with antibodies specific to Bud23 and Trm112. (*D*) Quantification of panels shown in *C*. Signals captured with the BioRad ChemiDoc MP imaging system. *x* axis, fractions 1–24; *y* axis, percent signal intensity for the indicated protein in each fraction.

transcript) and that it escorts pre-40S precursors into the cytoplasm (17), we determined the distribution of Bud23 and Trm112 on velocity gradients to assess the impact of selected mutations on the dynamics of recruitment of the Bud23–Trm112 complex to pre-ribosomes (Fig. 2 *C* and *D* and Fig. S4*D*). As a control, to inactivate Bud23 MTase function, we mutated the strictly conserved D77 residue, which forms hydrogen bonds with the SAM ribose 2′ and 3′ hydroxyl groups (Fig. 1*B*), into Ala (D77A), as previously done for other MTases (9, 31). Five mutants were stably expressed in yeast (Y22A, E18A, K21E/R27E, W122A, and Y159A) and, with the exception of E18A, all were enzymatically inactive in vivo

while retaining SAM binding activity in vitro (Table 1 and Fig. S2 *B* and *C*). Yeast cells expressing these five mutations had a normal doubling time and normal rRNA production (Table 1 and Fig. S2*A*). Like WT Bud23, the Y22A, W122A, and Y159A mutants predominantly colocalized with pre-90S ribosomes (fractions 10–12), with limited amounts in the lighter fractions (fractions 1–6; Fig. 2 *C* and *D* and Fig. S4*D*). Importantly, Trm112 comigrated partially with pre–90S-bound Bud23, indicating that the MTase is integrated within pre-ribosomes as a heterodimeric Bud23–Trm112 complex. Trm112 was also abundantly detected in lighter fractions, consistently with its known involvement in other complexes,

smaller in size, involved in tRNA (with Trm9 and Trm11) and translation factor (with Mtq2) modifications (see the introduction). In cells expressing the K21E/R27E mutation, most of the Bud23, and concomitantly of Trm112, was detected in lighter fractions of the gradient (peak centered around fraction 7), supporting a role for these positively charged residues in the interaction with the 18S rRNA phosphate backbone; this is consistent with the observed methylation inhibition (Table 1) and, as predicted above, indicates deficient pre-ribosome recruitment.

The four other mutants (I31W, D77A, S118E, and S118R) showed a decrease in protein level (from two- to fivefold) accompanied by loss of SAM binding and loss of enzymatic activity (Fig. S2 B and C and Table 1). Neither growth nor rRNA syn-thesis was affected in D77A, confirming that Bud23 MTase activity is fully dispensable for 18S rRNA production, whereas the presence of the protein is required (8); this is similar to what has been reported for other small ribosomal subunit base MTases (Dim1 and Emg1/Nep1) (7–9). Because I31 and S118 were found to have lost their ability to interact directly with SAM, we propose that these substitutions induce protein misfolding. In agreement with this view, I31W and S118E showed impaired growth and diminished protein stability. S118R proved quite stable, did not affect growth, and showed an increased level of association with large pre-90S ribosomes compared with wild-type protein (Fig. 2 C and D and Fig. S2 A and B). Again, the distribution of Trm112 strikingly matched that of Bud23, and the
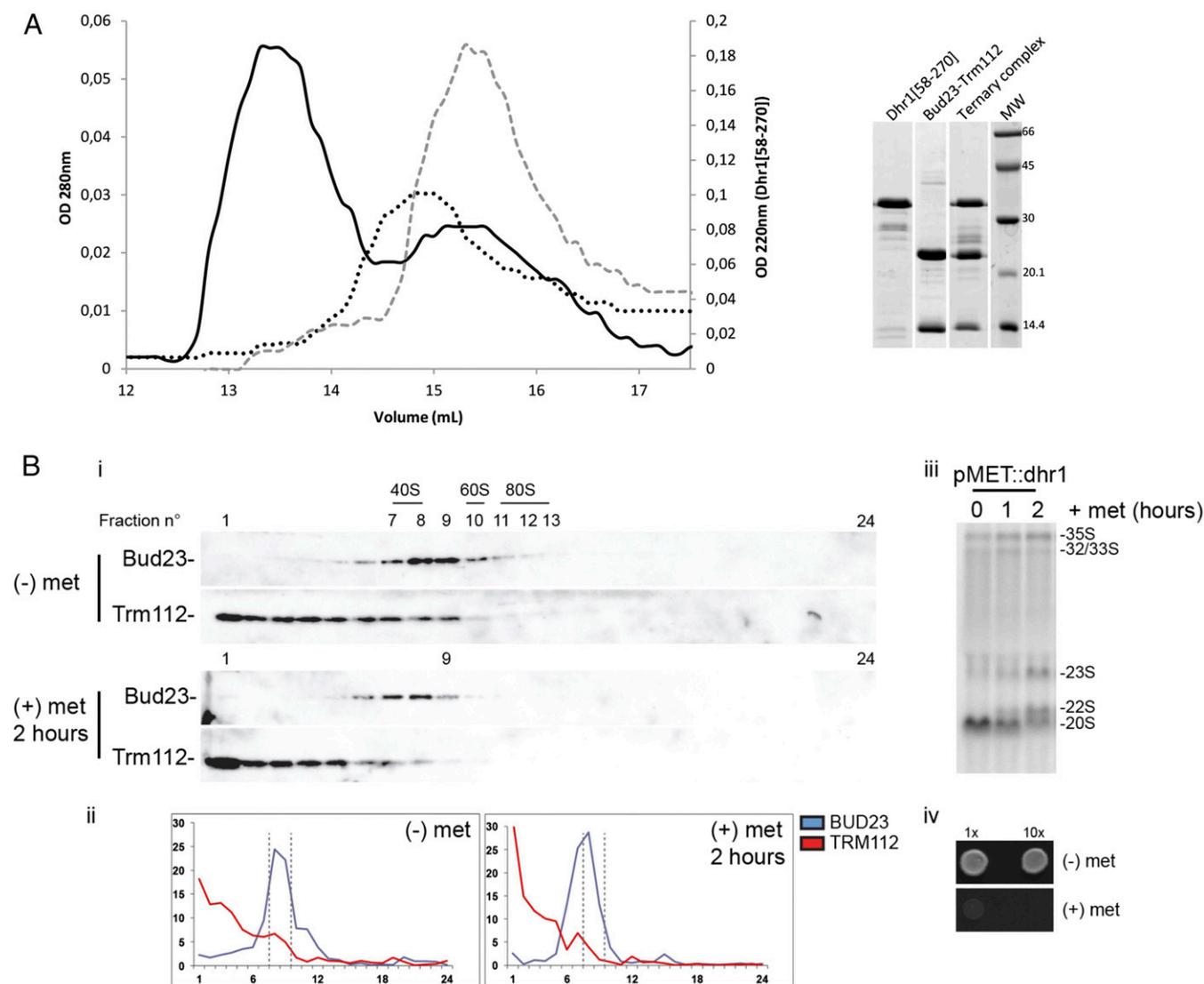
Fig. 3. Bud23–Trm112 complex interacts directly with Dhr1. (A, Left) Superposition of three different gel filtration elution profiles: Bud23–Trm112 complex alone (OD signal at 280 nm, black dotted line), Dhr1[58–270] alone (OD signal at 220 nm, gray dashed line), and the Bud23–Trm112–Dhr1[58–270] ternary complex after in vitro reconstitution (addition of Dhr1 to Bud23–Trm112, OD signal at 280 nm, black solid line). Black solid line, the minor peak observed (volume 15–16 mL) corresponds to the excess of Dhr1 [58–270] used to reconstitute the ternary complex. (Right) Analysis of the content of the major elution peak observed for each experiment on a 15% SDS/PAGE. MW, molecular weight marker. (B) The distribution of Bud23–Trm112 in velocity gradients is affected upon alteration of Dhr1 expression. (i and ii) Sucrose gradient analysis (Fig. 2) of total extracts of pMET::dhr1 cells grown in the absence or presence of me-thionine (met). The same amount of total extract, according to the OD_{260}, was loaded on each gradient. All Western blot membranes were exposed to film under the same conditions (i), or the luminescent signal was quantitated with a ChemiDoc (BioRad) and expressed as a percentage detected in each fraction (ii). (iii) Depletion of Dhr1 leads to inhibition of pre-rRNA processing at sites A_1 and A_2, with concomitant accumulation of aberrant 22S RNA. Total RNA extracted from pMET::dhr1 cells grown in the absence or presence of methionine for time points indicated was analyzed by Northern blotting with a probe specific to ITS1 (oligo b; Fig. 4B). (iv) Drop assay (1x and 10x dilution) on synthetic medium containing methionine or not. Cells were grown for 3 d at 30 °C.

heavier fractions were clearly enriched in Trm112. We speculate that the higher stability of S118R compared with S118E results from increased affinity for pre-90S, the mutation contributing a positively charged side chain contacting the rRNA phosphate backbone; this leads to retention of Bud23/Trm112 on nucleolar pre-ribosomes for an extended time. Because the S118R mutant behaves like the SAM binding-deficient D77A mutant (Table 1 and Fig. 2 *C* and *D*), this further suggests that SAM binding to Bud23–Trm112 influences its affinity for the pre-ribosome but does not interfere with correct 18S rRNA maturation.

Bud23–Trm112 and the DEAH Box Helicase Dhr1 Form a Ternary Complex.
The DEAH box RNA helicase Dhr1 and Bud23–Trm112 are part of the same pre-ribosomes (17). Further, a Dhr1 domain spanning residues [195–252] interacts with Bud23 in a two-hybrid assay (24). We expressed and purified a recombinant Dhr1 fragment consisting of residues 58–270 and analyzed its ability to interact directly with Bud23–Trm112 in vitro. Size-exclusion chromatography experiments demonstrated that Dhr1 [58–270] interacts stably with Bud23–Trm112, forming a heterotrimeric complex (Fig. 3*A*). Because our Bud23 construct extends from residue 1–202, this further indicates that residues 203–275 are dispensable for interaction with Trm112 and Dhr1. The helicase Dhr1 interacts tightly with the box C/D snoRNA U3 (25), which associates through Watson–Crick base-pairing with pre-rRNAs regulating the timing of central pseudoknot formation. The central pseudoknot is a long-range interaction occurring between residues located >1.1 kb apart on 18S rRNA; its formation is essential to the overall folding of small subunit rRNA. In maturing subunits, sequences base-paired in the pseudoknot are sequestered by interactions with U3. Dhr1 is suggested to trigger U3 displacement, a prerequisite to central pseudoknot formation (25).

Given the physical proximity of Dhr1 and Bud23–Trm112, we wondered if Dhr1 might be involved in structural rearrangements within pre-ribosomes that might contribute to efficient recruitment of Bud23–Trm112. We therefore established the distribution of Bud23–Trm112 on velocity gradients in the presence and absence of the helicase (Fig. 3*B*). We used a strain in which the endogenous promoter of *DHR1* was replaced directly on the chromosome by a methionine-regulated expression cassette (*pMET*). In this strain (*pMET::dhr1*), the expression of *DHR1* is rapidly "switched off" upon addition of methionine to the growth medium; this leads to the previously described inhibition of pre-rRNA processing at sites A_1 and A_2 and to accumulation of aberrant 22S RNA (Fig. 3*B*) (25). In *pMET::dhr1*, markedly reduced amounts of Bud23–Trm112 were found to comigrate with large nucleolar pre-90S ribosomes (Fig. 3*B*). A shift to lighter fractions was particularly obvious upon addition
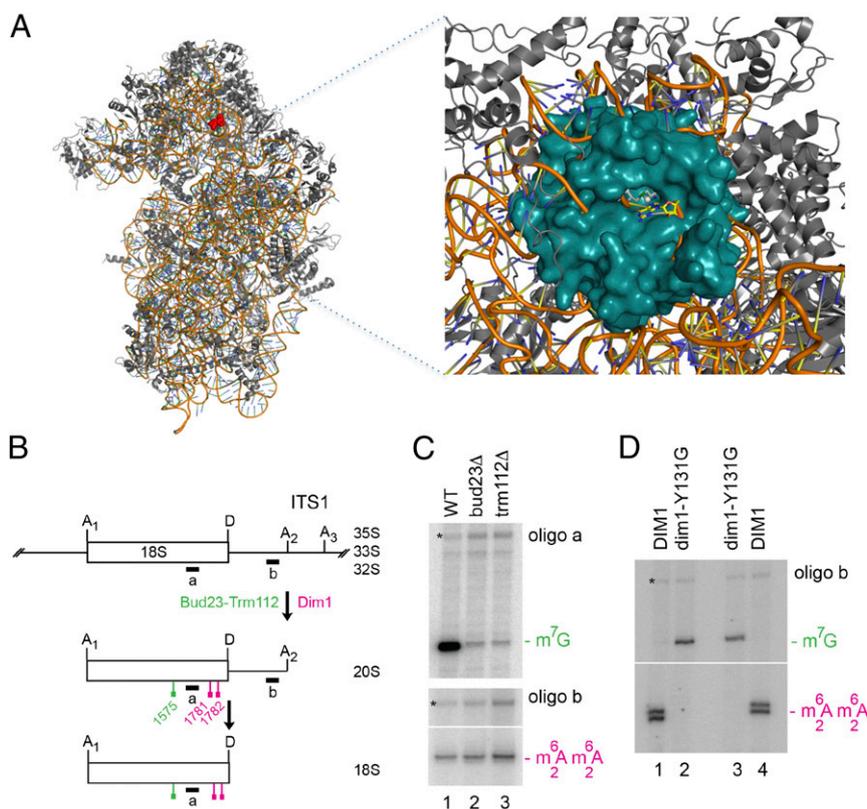
Fig. 4. m^{7}G methylation is a late maturation event occurring on 3′-extended 18S rRNA precursors. (*A*) Mature yeast 40S ribosomal subunit (PDB ID codes 3U5B and 3U5C) with G1575 highlighted in red; ribosomal proteins in gray; 18S rRNA in orange. (*Inset*) Superimposition of Bud23–Trm112–GMP model (blue) on G1575 (yellow sticks) in 40S reveals major steric clashes. (*B*) Simplified 18S rRNA synthesis pathway showing pre-rRNA intermediates (35S, 33S, 32S and 20S), cleavage sites (A_1, A_2, A_3, and D), oligonucleotides a and b, and the positions and timing of the m^{7}G$_{1575}$ and $m_2^6A_{1781}m_2^6A_{1782}$ modifications. (*C* and *D*) Primer extension mapping of m^{7}G$_{1575}$ and $m_2^6A_{1781}m_2^6A_{1782}$. Total RNA extracted from the strains indicated was processed for primer extension analysis with oligonucleotide a or b. For m^{7}G detection, total RNA was first cleaved at the site of modification by NaBH$_4$/aniline treatment (17). For m_2^6A detection, total RNA was directly subjected to primer extension (7). Lanes 1–2 and 3–4 in *D* show two independent biological replicates. Structural stops (*) indicate that gel loading was even. (*C*) m^{7}G$_{1575}$ is strictly dependent on Bud23 and Trm112. Dim1 dimethylation at A1781/A1782 requires neither Bud23 nor Trm112. (*D*) In wild-type cells (lanes 1 and 4), the presence of $m_2^6A_{1781}m_2^6A_{1782}$ on 20S pre-rRNA precludes detection of m^{7}G$_{1575}$ from primer b because the reverse transcriptase cannot get across position 1781/1782. The m^{7}G modification is detected only in catalytically deficient dim1 cells (dim1-Y131G, lanes 2 and 3). Pre-rRNAs selected by primer b on total RNA include 20S, 32S, 33S, and 35S. Because 32S, 33S, and 35S are naturally nondimethylated and because no m^{7}G signal is detected in lanes 1 and 4, we conclude that m^{7}G takes place at the level of 20S pre-rRNAs.

of methionine for 2 h, but it was also seen under permissive conditions, indicating that even in the absence of methionine, the expression of *DHR1* is affected owing to promoter replacement. The altered distribution of Bud23–Trm112 observed in *pMET::dhr1* is similar to that observed with mutation K21E/R27E, located in the proposed surface of interaction with pre-ribosomes, leading us to conclude that Dhr1 contributes to efficient recruitment of Bud23–Trm112 to pre-ribosomes.

m^7G_{1575} Is a Late Maturation Event Occurring on 3′-Extended 18S rRNA Precursors.

The superimposition of the Trm112-Bud23-GMP model onto residue G1575 in the crystal structure of the *S. cerevisiae* 80S ribosome (36) revealed important steric clashes between Bud23 and ribosomal components (Fig. 4*A*), suggesting that methylation occurs on precursors rather than on mature 18S rRNA. To test this prediction, we established the timing of methylation by differential primer extension, using oligonucleotides complementary to 18S rRNA (primer a), or internal transcribed spacer 1 (ITS1; primer b; Fig. 4*B*). All primer extensions were performed on total RNA.

To map m^7G by primer extension, total RNA was cleaved specifically at the site of modification by reduction with sodium borohydride followed by aniline treatment (17). With this method, m^7G_{1575} methylation was detected from primer a and, as expected, was lost in *bud23Δ* and *trm112Δ* cells (Fig. 4*C*) (17). To establish a modification timetable, we used as a reference $m_2^6A_{1781}m_2^6A_{1782}$ introduced by Dim1 at the 3′ end of 18S rRNA and previously established to occur at the level of 20S pre-rRNA (7). As expected, $m_2^6Am_2^6A$ was detected with primer b (Fig. 4*C*). In contrast to m^7G, mapping $m_2^6Am_2^6A$ by primer extension does not require any treatment of the RNA before cDNA synthesis, because it is a "bulky" modification, which blocks reverse transcriptase progression, producing a "stutter" (visible as a doublet) and eventually polymerase drop-off (7, 17, 19; further discussed in ref. 37). $m_2^6Am_2^6A$ was detected in cells lacking Bud23 or Trm112 (Fig. 4*C*), incidentally demonstrating that Dim1 dimethylation is not dependent upon prior m^7G_{1575} modification by Bud23–Trm112. Technically, the m^7G modification cannot be detected from primer b on 20S pre-rRNA because the Dim1-dependent dimethylation at A1781 and A1782 blocks the reverse transcriptase before it reaches G1575 (Fig. 4*D*, lanes 1 and 4). However, in cells expressing the catalytically deficient allele dim1-Y131G as their sole source of Dim1, m^7G_{1575} became detectable by primer extension from oligonucleotide b (Fig. 4*D*, lanes 2 and 3); this demonstrates that among the RNAs selected by primer b, which include the 35S, 33S, 32S, and 20S pre-rRNAs, some are m^7G methylated. Incidentally, this observation also demonstrates that m^7G is not dependent on prior dimethylation by Dim1. Because the 32S, 33S, and 35S are naturally nondimethylated pre-rRNA species, and because they did not appear to be m^7G methylated in our assay (Fig. 4*D*, lanes 1 and 4), we conclude that m^7G_{1575} occurs at the level of 20S pre-rRNA. In conclusion, Bud23–Trm112 and Dim1 are both active at the level of 20S pre-rRNA and they operate independently of each other.

Conclusions

In this work, we present crystal structures of yeast Bud23–Trm112 complexes in the apo and SAM-bound forms, revealing essential aspects of methylation catalysis, coactivation by Trm112 and ribosomal substrate recognition. We show that Trm112 undergoes an induced fit to accommodate its MTase partners. We confirm our earlier prediction that Bud23 associates with Trm112 through formation of a parallel β-zipper involving hydrogen bonds between main-chain atoms and masking a large, destabilizing hydrophobic surface on Bud23 (17). Together with the structure of the Mtq2–Trm112 complex (31), the Bud23–Trm112 structure highlights the extraordinary structural plasticity allowing Trm112 to interact with four MTases harboring less than

20% overall sequence identity. Bud23, Mtq2, Trm9, and most likely Trm11 use the same region of their class I SAM-dependent MTase fold, and strikingly similar types of interactions, to bind to the same region of their activator Trm112.

In addition, we identify residues important for Bud23–Trm112 complex formation, SAM binding, methyl transfer, and association with pre-ribosomes. We have modeled the catalytic pocket of Bud23, concluding that it coordinates its substrate in a fashion similar to *C. canephora* xanthosine MTase, with the guanosine aligned for methyl transfer according to an inline S_N2-type catalysis, typical of class I MTases.

When Does m^7G_{1575} Take Place?

Bud23 binds pre-ribosomes at an early nucleolar stage (17); nonetheless, we show that modification is specifically delayed, occurring at a late step in ribosome biogenesis, corresponding to 20S pre-rRNA formation and implying specific catalytic activation. What triggers this specific MTase activation is not currently understood. We discuss above the substrate accessibility issues within the Bud23–Trm112 catalytic cavity. Presumably, subunit biogenesis has to achieve a specific maturation stage such that substrate folding becomes compatible with RNA modification. We report that Bud23–Trm112 interacts directly with the DEAH box helicase Dhr1, forming a trimeric complex in vitro and requiring the latter's intervention for efficient recruitment to pre-ribosomes. Dhr1 is suggested to regulate the timing of central pseudoknot formation (25), a dramatic, irreversible structural reorganization absolutely essential to overall folding of small subunit RNA. Whether Bud23–Trm12 contributes to efficient central pseudoknot formation is under investigation.

Bud23–Trm112 displays striking structural similarity to *E. coli* RlmA^I, which catalyzes N^1-guanine base methylation on 23S rRNA ([Fig. S5](#)). RlmA^I is composed of an N-terminal zinc-binding domain juxtaposed to a class I MTase domain. In Bud23–Trm112, interestingly, the zinc-binding domain of Trm112 occupies precisely *in trans* the position of a similar domain present in *cis* in RlmA^I, with the zinc atom similarly located in the two structures ([Fig. S5](#)). Because the zinc-binding domain of RlmA^I is proposed to interact with 23S rRNA (38), we suggest that Trm112 might contribute to rRNA binding. The observation that Trm112 systematically comigrates with pre-ribosome-associated Bud23 is compatible with this possibility (Figs. 2 *C* and *D* and 3*B*) (17).

The function of the 18S rRNA m^7G_{1575} methylation in ribosome biogenesis and translation is not yet fully understood. Deletion of *BUD23* confers hypersensitivity to paromomycin and a cold-sensitive growth defect ([Fig. S6](#)). However, methylation per se is not required for optimal growth because cells expressing catalytically defective *bud23* alleles exhibit normal growth (Table 1) (8). We believe it very unlikely that cells would have evolved and conserved such a sophisticated modification mechanism, involving formation of the Bud23–Trm112 heterodimeric holoenzyme and delayed modification, if m^7G_{1575} did not confer any advantages for ribosome biogenesis or function. On the small subunit, m^7G is precisely located at a ridge forming a steric block between the P- and E-site tRNAs, compatible with a possible function during protein synthesis. For comparison, Dim1 is essential to cell survival because it is required for early nucleolar pre-rRNA processing steps indispensable for 18S rRNA synthesis, whereas the $m_2^6A_{1781}m_2^6A_{1782}$ dimethylation is not essential to growth, and cells expressing a catalytically deficient methylation allele of *DIM1* are perfectly viable (7, 19). However, yeast cells expressing nondimethylated ribosomes are hypersensitive to aminoglycoside antibiotics and impaired for in vitro translation of specific mRNAs (19); this indicates that the modification does play a significant role in translation.

Finally, WBSCR22, the human Bud23 ortholog, is highly expressed in invasive breast cancers, and the integrity of its SAM binding motif is required to confer metastatic properties to otherwise nonmetastatic cells (28). Furthermore, silencing of WBSCR22

results in specifically increased lethality of myeloma cells, identifying it as a potential target for cancer therapy (29). By uncovering absolutely essential observations on Bud23–Trm112 catalysis and substrate interaction, this work contributes decisive novel elements to the molecular characterization of human disease symptoms associated with ribosome biogenesis dysfunction caused by WBSCR22 malfunction.

1. Woolford JL, Jr, Baserga SJ (2013) Ribosome biogenesis in the yeast *Saccharomyces cerevisiae*. *Genetics* 195(3):643–681.
2. Henras A, Plisson-Chastang C, O'Donohue M-F, Chakraborthy A, Gleizes P-E (2014) Overview of pre-rRNA processing in eukaryotes. *WIREs RNA*, 10.1002/wrna.1269.
3. Thomson E, Ferreira-Cerca S, Hurt E (2013) Eukaryotic ribosome biogenesis at a glance. *J Cell Sci* 126(Pt 21):4815–4821.
4. Lafontaine DLJ, Non-coding RNAs in eukaryotic ribosome synthesis and function. *Nat Struct Mol Biol* 21, in press.
5. Motorin Y, Helm M (2011) RNA nucleotide methylation. *Wiley Interdiscip Rev RNA* 2(5):611–631.
6. Watkins NJ, Bohnsack MT (2012) The box C/D and H/ACA snoRNPs: Key players in the modification, processing and the dynamic folding of ribosomal RNA. *Wiley Interdiscip Rev RNA* 3(3):397–414.
7. Lafontaine D, Vandenhaute J, Tollervey D (1995) The 18S rRNA dimethylase Dim1p is required for pre-ribosomal RNA processing in yeast. *Genes Dev* 9(20):2470–2481.
8. White J, et al. (2008) Bud23 methylates G1575 of 18S rRNA and is required for efficient nuclear export of pre-40S subunits. *Mol Cell Biol* 28(10):3151–3161.
9. Leulliot N, Bohnsack MT, Graille M, Tollervey D, Van Tilbeurgh H (2008) The yeast ribosome synthesis factor Emg1 is a novel member of the superfamily of alpha/beta knot fold methyltransferases. *Nucleic Acids Res* 36(2):629–639.
10. Ishitani R, Yokoyama S, Nureki O (2008) Structure, dynamics, and function of RNA modification enzymes. *Curr Opin Struct Biol* 18(3):330–339.
11. Schubert HL, Blumenthal RM, Cheng X (2003) Many paths to methyltransfer: A chronicle of convergence. *Trends Biochem Sci* 28(6):329–335.
12. Peifer C, et al. (2013) Yeast Rrp8p, a novel methyltransferase responsible for m1A 645 base modification of 25S rRNA. *Nucleic Acids Res* 41(2):1151–1163.
13. Sharma S, et al. (2014) Identification of novel methyltransferases, Bmt5 and Bmt6, responsible for the m3U methylations of 25S rRNA in *Saccharomyces cerevisiae*. *Nucleic Acids Res* 42(5):3246–3260.
14. Sharma S, Yang J, Watzinger P, Kötter P, Entian KD (2013) Yeast Nop2 and Rcm1 methylate C2870 and C2278 of the 25S rRNA, respectively. *Nucleic Acids Res* 41(19):9062–9076.
15. Sharma S, Watzinger P, Kötter P, Entian KD (2013) Identification of a novel methyltransferase, Bmt2, responsible for the N-1-methyl-adenosine base modification of 25S rRNA in *Saccharomyces cerevisiae*. *Nucleic Acids Res* 41(10):5428–5443.
16. Meyer B, et al. (2011) The Bowen–Conradi syndrome protein Nep1 (Emg1) has a dual role in eukaryotic ribosome biogenesis, as an essential assembly factor and in the methylation of Ψ1191 in yeast 18S rRNA. *Nucleic Acids Res* 39(4):1526–1537.
17. Figaro S, et al. (2012) Trm112 is required for Bud23-mediated methylation of the 18S rRNA at position G1575. *Mol Cell Biol* 32(12):2254–2267.
18. Sardana R, White JP, Johnson AW (2013) The rRNA methyltransferase Bud23 shows functional interaction with components of the SSU processome and RNase MRP. *RNA* 19(6):828–840.
19. Lafontaine DLJ, Preiss T, Tollervey D (1998) Yeast 18S rRNA dimethylase Dim1p: A quality control mechanism in ribosome synthesis? *Mol Cell Biol* 18(4):2360–2370.
20. Heurgué-Hamard V, et al. (2006) The zinc finger protein Ynr046w is plurifunctional and a component of the eRF1 methyltransferase in yeast. *J Biol Chem* 281(47):36140–36148.
21. Mazauric MH, Dirick L, Purushothaman SK, Björk GR, Lapeyre B (2010) Trm112p is a 15-kDa zinc finger protein essential for the activity of two tRNA and one protein methyltransferases in yeast. *J Biol Chem* 285(24):18505–18515.
22. Purushothaman SK, Bujnicki JM, Grosjean H, Lapeyre B (2005) Trm11p and Trm112p are both required for the formation of 2-methylguanosine at position 10 in yeast tRNA. *Mol Cell Biol* 25(11):4359–4370.
23. Phipps KR, Charette J, Baserga SJ (2011) The small subunit processome in ribosome biogenesis—progress and prospects. *Wiley Interdiscip Rev RNA* 2(1):1–21.
24. Sardana R, Zhu J, Gill M, Johnson AW (2014) Physical and functional interaction between the methyltransferase Bud23 and the essential DEAH-box RNA helicase Ecm16. *Mol Cell Biol* 34(12):2208–2220.
25. Colley A, Beggs JD, Tollervey D, Lafontaine DLJ (2000) Dhr1p, a putative DEAH-box RNA helicase, is associated with the box C+D snoRNP U3. *Mol Cell Biol* 20(19):7238–7246.
26. Õunap K, Käsper L, Kurg A, Kurg R (2013) The human WBSCR22 protein is involved in the biogenesis of the 40S ribosomal subunits in mammalian cells. *PLoS ONE* 8(9):e75686.
27. Tafforeau L, et al. (2013) The complexity of human ribosome biogenesis revealed by systematic nucleolar screening of Pre-rRNA processing factors. *Mol Cell* 51(4):539–551.
28. Nakazawa Y, Arai H, Fujita N (2011) The novel metastasis promoter Merm1/Wbscr22 enhances tumor cell survival in the vasculature by suppressing Zac1/p53-dependent apoptosis. *Cancer Res* 71(3):1146–1155.
29. Tiedemann RE, et al. (2012) Identification of molecular vulnerabilities in human multiple myeloma cells by RNA interference lethality screening of the druggable genome. *Cancer Res* 72(3):757–768.
30. Doll A, Grzeschik KH (2001) Characterization of two novel genes, WBSCR20 and WBSCR22, deleted in Williams–Beuren syndrome. *Cytogenet Cell Genet* 95(1-2):20–27.
31. Liger D, et al. (2011) Mechanism of activation of methyltransferases involved in translation by the Trm112 'hub' protein. *Nucleic Acids Res* 39(14):6249–6259.
32. Holm L, Rosenstrom P (2010) Dali server: Conservation mapping in 3D. *Nucleic Acids Res* 38(Web Server issue):W545–549.
33. Schmitt E, Galimand M, Panvert M, Courvalin P, Mechulam Y (2009) Structural bases for 16 S rRNA methylation catalyzed by ArmA and RmtB methyltransferases. *J Mol Biol* 388(3):570–582.
34. Fabrega C, Hausmann S, Shen V, Shuman S, Lima CD (2004) Structure and mechanism of mRNA cap (guanine-N7) methyltransferase. *Mol Cell* 13(1):77–89.
35. McCarthy AA, McCarthy JG (2007) The structure of two N-methyltransferases from the caffeine biosynthetic pathway. *Plant Physiol* 144(2):879–889.
36. Ben-Shem A, et al. (2011) The structure of the eukaryotic ribosome at 3.0 Å resolution. *Science* 334(6062):1524–1529.
37. Motorin Y, Muller S, Behm-Ansmant I, Branlant C (2007) Identification of modified residues in RNAs by reverse transcription-based methods. *Methods Enzymol* 425:21–53.
38. Das K, et al. (2004) Crystal structure of RlmAI: Implications for understanding the 23S rRNA G745/G748-methylation at the macrolide antibiotic-binding site. *Proc Natl Acad Sci USA* 101(12):4041–4046.
39. Martin JL, McMillan FM (2002) SAM (dependent) I AM: The S-adenosylmethionine-dependent methyltransferase fold. *Curr Opin Struct Biol* 12(6):783–793.